A Tutorial on Frequency Stability Fundamentals

Haziq Rohail and David C. Burnett
Department of Electrical and Computer Engineering, Portland State University, Portland, Oregon, USA
haziq@pdx.edu, dburnett@pdx.edu

***Abstract*—Local Oscillator (LO) stability is paramount for optimal performance in RF communication systems. Frequency fluctuations in the LO can not only result in reciprocal mixing in narrowband communication systems, but it can also cause carrier mismatches between the transmitter and receiver, resulting in higher guard times and Bit Error Rates (BER); even in the absence of adjacent channels. While traditional communication systems rely on high-quality crystal oscillators and Phase-Locked Loops (PLLs) to maintain frequency stability, the power and area constraints, and sometimes battery-less nature of IoT motes urge the elimination of the crystal reference and PLL. Consequently, there is a growing demand for low-power oscillators that are stable enough to meet the requirements of modern communication standards such as IEEE 802.15.4 and Bluetooth Low Energy (BLE). The stability of an oscillator's frequency can be evaluated in both frequency and time domains using metrics such as phase noise, jitter, and Allan variance. This tutorial paper provides a comprehensive summary of the key metrics employed in the measurement of frequency stability, along with their conversion methods. By elucidating these critical measures, this paper aims to enhance understanding and facilitate the designers to better comprehend the subtle nuances of frequency stability.**

***Index Terms*—phase noise, jitter, RF oscillators, Allan variance**

I. Introduction

The goal of crystal-free IoT devices is to eliminate the need for the crystal reference and Phased Lock Loop (PLL) in order to reduce the power consumption and area utilization of IoT devices. By eliminating the crystal reference and only using free-running on-chip oscillators for both time keeping and RF communication, the power consumption of the IoT mote may be reduced significantly. To that end, low-power on-chip oscillators that can satisfy the frequency stability/phase noise criteria of communication standards such as IEEE 802.15.4 [1] and Bluetooth Low Energy (BLE) [2] are needed. Due to the phase/frequency fluctuations in the oscillator's output, the frequency spectrum of the oscillator shows sidebands around its fundamental frequency and its multiples [3]. The presence of these phase noise sidebands in the oscillator's spectrum has a direct impact on the performance of the entire communication system. It causes the undesired out of band frequency contents to get converted into the same IF band as the operating frequency, in a process called reciprocal mixing. In such a scenario, if the undesired signal is stronger than the desired one, it can result in masking and degrade the receiver's performance [4]. Furthermore, frequency drift of a free-running oscillator may also cause carrier and symbol rate mismatches between the transmitter and receiver even in the absence of adjacent channels; which may increase the guard time needed as well as the Bit Error Rate (BER). Therefore, ensuring the frequency stability of the free-running LO in crystal free motes is paramount [5], and these requirements become especially stringent for narrowband communication systems.

The ideal oscillator with a sinusoidal output generates a single tone $V_0 cos(2\pi v_0 t + \phi)$ and its spectrum contains only a single impulse at $\omega_0 = 2\pi v_0$. However, the output signal of a practical oscillator contains both voltage and time fluctuations, and can be expressed as given in (1), wherein, $\epsilon(t)$ represents the voltage fluctuations and $\phi(t)$ represents the phase fluctuations or frequency instabilities [6]. Note here that the center frequency v_0 in (1) may also be represented as f_0 in some modern texts. Similarly, the instantaneous frequency $v(t)$ may be represented as $f(t)$. They will be used interchangably in this text. In most modern oscillator designs, amplitude fluctuations $\epsilon(t)$ are negligible. The phase/frequency fluctuations $\phi(t)$, on the other hand, are more significant and hard to control.

$$V(t) = (V_0 + \epsilon(t))cos(2\pi v_0 t + \phi(t)) \tag{1}$$

Generally speaking, a crystal oscillator is used as a reference and a Phased Locked Loop (PLL) is locked to this reference to achieve the desired phase noise characteristics. However, the crystal oscillator requires a relatively large amount of power and area, which are both limited resources, especially in Internet of Things (IoT) motes. Furthermore, due to the high Quality factor (Q), crystal oscillators also require a significant warm-up time, ($\approx 0.5 - 5ms$) in the case of typical crystal oscillators, or ($\approx 20 - 400\mu s$) in the case of ones that use a fast start-up technique [7]. The high startup time increases the time required from wake-up to receiver listening which also leads to undesired power wastage.

On-chip LC oscillators, and relaxation oscillators such as Resistor Capacitor (RC) Oscillators and Ring Oscillators (ROs) are potential alternatives to the crystal oscillator [8]–[10]. Among these options, relaxation oscillators, and especially ROs, require exceptionally low power and area but suffer from poor frequency stability and high phase noise [11]–[13]. The frequency response of relaxation oscillators is generally monotonic, as shown in Fig. 1(a), as opposed to that of LC oscillators shown in Fig. 1(b). The bell-shaped magnitude response, and the sharp transition in the phase response, of the transfer function of LC oscillator results from the opposite nature of the impedance of the inductive and capacitive elements. At frequencies below resonance, the inductive impedance dominates and gives an increasing impedance profile, whereas, at frequencies above resonance, the capacitive impedance

979-8-3503-6330-2/24/$31.00 ©2024 IEEE
DOI 10.1109/CrystalFreeIoT62484.2024.00005

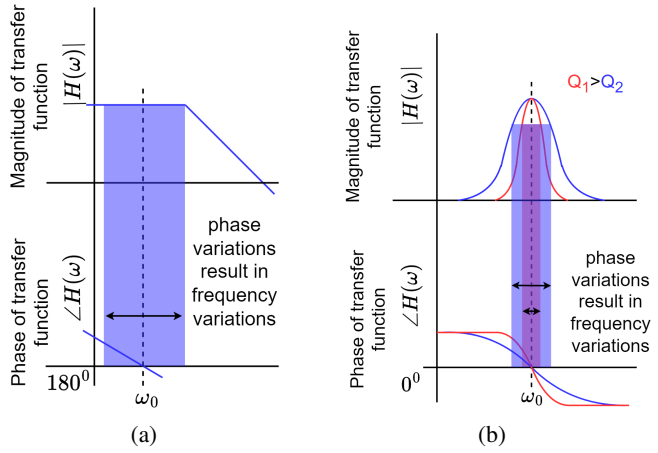

Fig. 1: Frequency response of (a) a typical relaxation oscillator, and (b) LC oscillators with different Q. LC oscillators have better sideband suppression, and hence, frequency stability.

dominates giving a decreasing profile. The LC oscillator's Q is defined as the ratio of the average energy stored to the energy lost per cycle, or $\frac{|Z_{im}|}{Z_{Re}} = \frac{\omega_0 L}{R}$ in the case of a simple series LC circuit. Oscillators with a high Q demonstrate a sharper transition as well as better phase noise characteristics [14]. This is primarily due to the fact that a higher quality factor results in higher suppression of harmonics and other out of band frequency content, and hence, improves the phase noise of the oscillator. This suppression happens in both magnitude and phase domains. The Barkhausen criteria proposes the necessary, though not sufficient, conditions for oscillations, stating that in order to sustain oscillations, the magnitude of the transfer function in a closed loop system must be greater than or equal to 1, and the phase change must be 360^0. Consider a frequency $\omega' = \omega_0 + \Delta\omega$, such that $\omega_0 >> \Delta\omega$. In the absence of noise, only ω_0 satisfies the oscillation criteria, and ω' does not contain any power. However, due to inherent noise in the circuit, such as due to supply noise, thermal and flicker noise of the devices, etc, both amplitude and phase fluctuations can occur, which can cause the circuit to oscillate at ω'. In such a case, a sharp transition in both amplitude and phase can help prevent the circuit, from oscillating at ω', or at least attenuate it to some extent. The sharp transition in phase, or in other words a high $\frac{d\angle H(\omega)}{d\omega}$, as can be seen in the case of LC oscillators, contributes by causing even the smallest shifts in ω to result in large changes in the phase $\angle H(\omega)$, thereby making it difficult for the circuit to satisfy the Barkhausen criteria [14] and suppressing the sideband power. However, in the case of relaxation oscillators, since they don't benefit from such a suppression due to the first order nature of their frequency response, these conditions can be met at a broad range of frequencies. Thus these types of oscillators are much more susceptible to noise, which results in poor frequency stability making them unsuitable for use in high performance RF front-ends with stringent phase noise requirements. A more rigorous analysis of oscillator noise is outside the scope of this paper but can be found in [3]. Though generally speaking, better frequency stability requires higher power consumption, careful manipulation of the oscillator's time-domain characteristics, such as waveform symmetry, and the shape of frequency response through Q in the case of resonant circuits, can allow designers to achieve the best frequency stability possible within a given power budget [3]. The frequency stability of oscillators can be quantified using a number of metrics. Oscillator jitter and phase noise are generally used to describe short term fluctuations, whereas, Allan deviation is used to describe long term fluctuations [15]. A sound understanding of these metrics is essential to be able to accurately quantify the frequency stability of oscillators. This paper reviews the key definitions used in frequency stability analysis, as well as their conversion methods, along with the power laws used to describe different noise processes that appear in oscillators.

II. Frequency Stability Measures

The frequency stability of oscillators and frequency synthesizers can be characterized in both time and frequency domain. The IEEE standard 1139-2022 [6] describes the key frequency and time domain methods used for characterizing frequency stability. Some of these are briefly discussed in this section.

A. Frequency Domain Measures

The quantities used to describe the oscillator's amplitude and frequency fluctuations in the frequency domain are discussed here. The instantaneous changes in normalized signal amplitude are termed fractional amplitude fluctuations $a(t)$ (2). Their one sided Power Spectral Density (PSD) known as the amplitude spectrum $S_a(f)$ is given in (6) and has units of $\frac{1}{Hz}$, wherein, $\langle a^2(f)\rangle$ is the mean of the square of the amplitude fluctuations $a(t)$ in the band Δf_k. The instantaneous changes in frequency are characterized using the normalized difference between instantaneous $v(t)$ and nominal v_0 frequencies, called the fractional frequency fluctuations $y(t)$, as given in (3). The one sided PSD of the fractional frequency fluctuations $y(t)$ is called $S_y(f)$. It too has units of $\frac{1}{Hz}$ and is given in (7), wherein, $\langle y^2(f)\rangle$ is the mean of the square of the fractional frequency fluctuations $y(t)$.

$$a(t) = \frac{|V(t)| - V_0}{V_0} = \frac{\epsilon(t)}{V_0} \tag{2}$$

$$y(t) = \frac{v(t) - v_0}{v_0} \tag{3}$$

From (1), $y(t)$ can also be expressed in terms of the phase fluctuations $\phi(t)$ as:

$$y(t) = \frac{1}{2\pi v_0}\frac{d\phi}{dt} \tag{4}$$

or, in terms of the time deviation, $x(t) = \frac{\phi}{2\pi v_0}$ as:

$$y(t) = \frac{x(t)}{dt} \tag{5}$$

The one sided PSD of the instantaneous phase fluctuations $\phi(t)$ is called phase spectrum $S_\phi(f)$, and one half of phase

spectrum $S_\phi(f)$ is called the phase noise $\mathcal{L}(f)$ (read as script L of f). Both $S_\phi(f)$ and $\mathcal{L}(f)$ have dimensions of squared angle over frequency $\frac{rad^2}{Hz}$. Due to historical reasons, they are typically expressed as a ratio of noise power to the power of the fundamental frequency in the units of $\frac{dBc}{Hz}$. $S_\phi(f)$ is given in (8) and $\mathcal{L}(f)$ is given in (9). The time spectrum $S_x(f)$ is the one sided PSD of the time fluctuations $x(t)$. It has units of $\frac{s^2}{Hz}$ and is given in (10).

$$S_a(f) = \frac{1}{\Delta f_k}\langle a^2(f)\rangle \tag{6}$$

$$S_y(f) = \frac{1}{\Delta f_k}\langle y^2(f)\rangle \tag{7}$$

$$S_\phi(f) = \frac{1}{\Delta f_k}\langle \phi^2(f)\rangle \tag{8}$$

$$\mathcal{L}(f) = \frac{1}{2}S_\phi(f) = \frac{1}{2\Delta f_k}\langle \phi^2(f)\rangle \tag{9}$$

$$S_x(f) = \frac{1}{\Delta f_k}\langle x^2(f)\rangle \tag{10}$$

Also, since frequency is the time derivative of phase, one can relate the spectral densities of phase and frequency as given in (11):

$$S_y(f) = (2\pi f)^2 S_x(f) = \frac{f^2}{v_0^2}S_\phi(f) = \frac{2f^2}{v_0^2}\mathcal{L}(f) \tag{11}$$

Among these measures, the phase noise $\mathcal{L}(f)$ is most commonly reported in the literature, typically as a function of frequency offset Δf from the nominal frequency f_0 [9], [16], [17]. In addition to phase noise, a Figure of Merit (FoM) [16], [18], [19] that also accounts for the power consumption of the oscillator is often reported:

$$FoM = 20\,log\Big(\frac{f_0}{\Delta f}\Big) - \mathcal{L}(\Delta f) - 10\,log\,P_{diss|mW} \tag{12}$$

wherein, f_0 is the center frequency, Δf is the frequency offset from f_0 where phase noise $\mathcal{L}(\Delta f)$ is measured, and $P_{diss|mW}$ is the power dissipated in units of milliwatts. The definition for FoM given in (12) results in a positive FoM, since $log\big(\frac{f_0}{\Delta f}\big)$ is positive and $\mathcal{L}(\Delta f)$ is negative. Another version that results in a negative FoM is also sometimes reported [12], [17], [20]. Note that the relative contributions of all three factors, and the resultant absolute value of FoM, are still the same.

B. Time Domain Measures

1) Jitter: Jitter and wander are used to express the variations of the zero crossing, or some other significant instant of a signal, from its ideal position. Jitter is used to express variations consisting of Fourier frequencies above 10 Hz and wander is used for variations with Fourier frequencies below 10 Hz [6]. Jitter can be measured in units of radians, seconds, or Unit Interval (UI), and it can be defined in multiple ways. Some of the most commonly used definitions from [21] are repeated here.

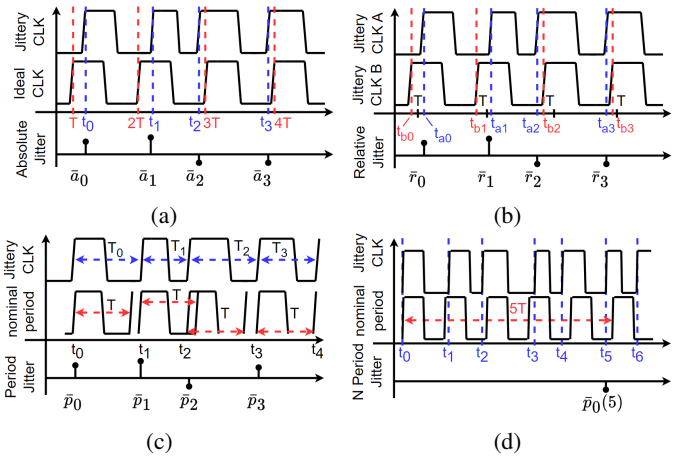

Fig. 2: Illustration of various jitter definitions adapted from [21]. (a) Absolute jitter, (b) relative jitter, (c) period jitter, and (d) N period jitter, with N=5.

a) Absolute Jitter: Absolute jitter is a discrete time sequence $\bar{a}$, such that each element $\bar{a}_k$ is the difference between the time instants of the zero crossings, either rising or falling, of the oscillator under test and an ideal reference oscillator. It is expressed as:

$$\bar{a}_k = t_k - kT \tag{13}$$

wherein, T is the ideal period, k is the number of oscillations, and t_k is the time instant of the k_{th} zero crossing. Two clock signals, an ideal clock and a non-ideal or jittery clock that is being compared to the ideal clock are shown in Fig. 2(a) [21]. The ideal clock's rising edges are always separated by the fixed period T, whereas, the rising edges of the jittery clock vary in time due to noise. The differences between the time instants of the rising edges of the two clocks are also shown in Fig. 2(a). Note that although Fig. 2 shows a square wave signal, these definitions of jitter can be applied to all sorts of periodic signals.

b) Relative Jitter: The discrete-time sequence obtained by comparing the oscillator under test to another non-ideal oscillator is called relative jitter $\bar{r}$, wherein, each element $\bar{r}_k$ is the difference between the time instants of the zero crossings of the oscillator under test and the non-ideal oscillator. The relative jitter of two non-ideal clocks CLK A and CLK B is shown in Fig. 2(b). This is a more practical measure since neither of the clocks has to be ideal. The relative jitter in terms of the absolute jitter of the two clocks is given as:

$$\bar{r}_k = t_{k(CLKA)} - t_{k(CLKB)} = \bar{a}_{k(CLKA)} - \bar{a}_{k(CLKB)} \tag{14}$$

c) Period/Cycle Jitter: Unlike the previous two types of jitter, period jitter $\bar{p}$, also known as cycle jitter Jc, compares the clock to itself by determining the variations in the period around its nominal value. It is more typically used in digital applications. The period jitter of a clock is shown in Fig. 2(c). It is the difference between the instantaneous period T_k of the clock under test and its nominal period T, and is given as:

$$\bar{p}_k = (t_{k+1} - t_k) - T = T_k - T = \bar{a}_{k+1} - \bar{a}_k \tag{15}$$

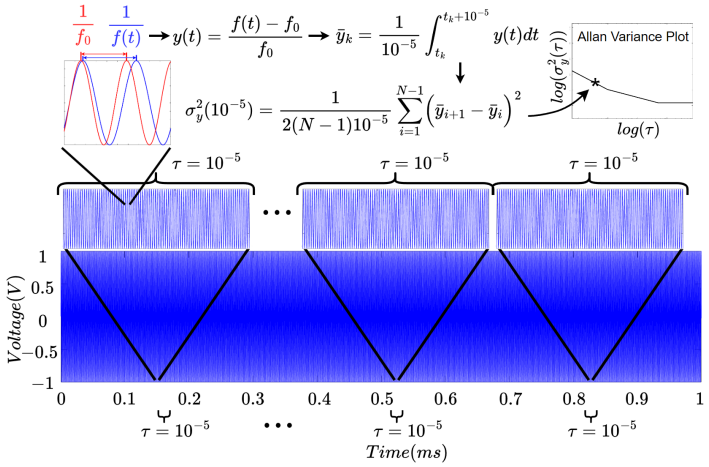

Fig. 3: Illustration of Allan Variance computation for a single value of $\tau = 10^{-5}$ that is shown as * in the inset. The process is repeated with different τ values to get the typical Allan Variance plot shown in the inset.

d) N-Period/Accumulated Jitter: Period jitter $\bar{p}$ can also be extended to N-period jitter $\bar{p}(N)$, also known as accumulated jitter, shown in Fig. 2(d) and given as:

$$\bar{p}_{k(N)} = (t_{k+N} - t_k) - NT = T_k - T = \bar{a}_{k+N} - \bar{a}_k \quad (16)$$

It compares the edge of the clock to another edge N periods apart from it. The N-period jitter can be written in terms of period jitter as:

$$\bar{p}_{k(N)} = \sum_{i=k}^{k+N-1} \bar{p}_i \quad (17)$$

2) Allan Variance: While phase noise and jitter measures are primarily associated with short-term frequency fluctuations, the long-term frequency stability may be measured using variance/deviation, specifically Allan variance $\sigma_y^2(t)$, commonly abbreviated as AVAR [22]:

$$\sigma_y^2(\tau) = \frac{1}{2}\langle[\bar{y}_{k+1} - \bar{y}_k]^2\rangle \quad (18)$$

wherein, the angle brackets $\langle\rangle$ denote average over infinite time, and $\bar{y}_k$ represents the average of the fractional frequency fluctuations $y(t)$ computed over an interval τ as:

$$\bar{y}_k = \frac{1}{\tau}\int_{t_k}^{t_k+\tau} y(t)dt \quad (19)$$

Thus according to (18), AVAR is half of the time average of the square of the difference between average fractional frequency fluctuations $\bar{y}_k$ over two adjacent time intervals of length τ. For a finite number of samples N, it can be computed as:

$$\sigma_y^2(\tau) = \frac{1}{2(N-1)}\sum_{i=1}^{N-1}\left(\bar{y}_{i+1} - \bar{y}_i\right)^2 \quad (20)$$

wherein, i denotes the number of measurements in a set of N samples that are τ seconds apart from each other. As the fractional frequency fluctuations $y(t)$ are dimensionless, so are their averages $\bar{y}_k$, and Allan variance. Since the fractional frequency fluctuations $y(t)$ are a derivative of the phase $x(t)$, Allan variance can also be computed using time deviation measurements $x(t)$ as:

$$\bar{y}_k = \frac{1}{\tau}\int_{t_k}^{t_k+\tau}\frac{dx(t)}{dt}dt \quad = \frac{1}{\tau}x(t)\Big|_{t_k}^{t_k+\tau} = \frac{x(t_k+\tau) - x(t_k)}{\tau} \quad (21)$$

Combining (21) and (18), and using $t_{k+1} = t_k + \tau$, we get:

$$\begin{aligned}\sigma_y^2(\tau) &= \left\langle \frac{1}{2\tau^2}\Big[\{x(t_{k+1}+\tau) - x(t_{k+1})\} \right.\\ &\quad \left. - \{x(t_k+\tau) - x(t_k)\}\Big]^2\right\rangle \\ &= \left\langle \frac{1}{2\tau^2}\Big[x(t_k+2\tau) + 2x(t_k+\tau) + x(t_k)\Big]^2\right\rangle \\ \Rightarrow \sigma_y^2(\tau) &= \left\langle \frac{1}{2\tau^2}\Big(x_{i+2} - 2x_{i+1} + x_i\Big)^2\right\rangle\end{aligned}$$

For a limited data set with N samples, this becomes:

$$\sigma_y^2(\tau) = \frac{1}{2(N-2)\tau^2}\sum_{i=1}^{N-2}\Big(x_{i+2} - 2x_{i+1} + x_i\Big)^2 \quad (22)$$

For the sake of the reader's comprehension, AVAR may be compared to the standard variance, in that AVAR first averages the fractional frequency fluctuations $y(t)$ over τ long windows, and then subtracts these adjacent averages. In contrast, standard variance would have directly subtracted the $y(t)$ values from a total sample mean of $y(t)$. This is done to remove the effects of frequency drift. If the average frequency of the oscillator drifts over time, and this drift is not removed, the sample mean fails to converge, and so does the standard variance. By comparing $\bar{y}_k$ values of adjacent time windows with each other, instead of comparing $y(t)$ values to the overall sample mean, AVAR removes the effect of this frequency drift. Furthermore, it also becomes a function of the averaging window length τ, instead of being a single scalar. An interesting consequence of this process is that the dependence of $\sigma_y^2(\tau)$ on τ is complementary to that of $S_y(f)$ on f. Since AVAR uses two samples of $\bar{y}_k$, it is also called two sample variance. The square root of AVAR $\sigma_y(\tau)$ is called Allan deviation (ADEV) or two sample deviation. The computation of AVAR for an interval $\tau = 10^{-5}s$ is illustrated in Fig. 3. The process shown in Fig. 3 is repeated for all desired τ values and the typical AVAR plot, on a log-log scale, shown in the inset is obtained.

Consider, for instance, a 1 second data set used for computing Allan variance. For a τ value of 10 ms, only 10 $\bar{y}_k$ samples would be available if only adjacent intervals are used. However, by using slightly smaller windows of size $\tau_0 = \frac{\tau}{m}$, with an averaging factor m, and overlapping the data within these windows, a better estimate can be achieved that uses not just adjacent but all possible τ intervals, called overlapping Allan variance as given in (23) [23]. In the previous case, if an averaging factor of $m = 3$ is used, overlapping Allan

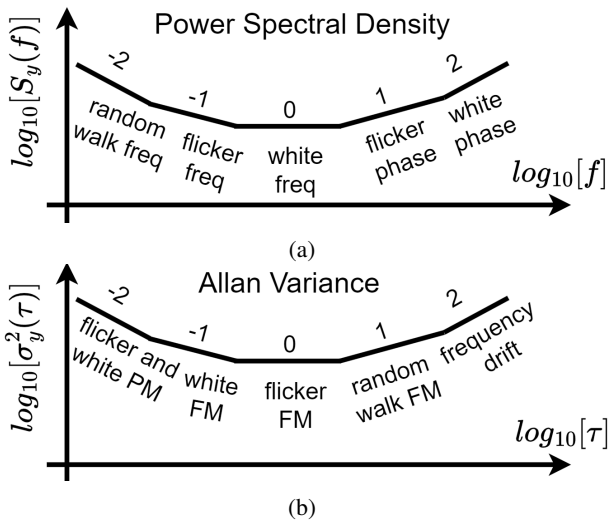

Fig. 4: Characteristic (a) Power Spectral Density (PSD) and (b) Allan Variance plots of different noise processes [6].

variance would result in $3 \times 10 - 2 = 28$ total samples, and hence, provides better smoothing of the results.

$$\sigma_y^2(\tau) = \frac{1}{2(N-2m)\tau^2} \sum_{i=1}^{N-2m} \Big(x_{i+2m} - 2x_{i+m} + x_i\Big)^2 \tag{23}$$

3) Modified Allan Variance: A modified version of the Allan variance $Mod\,\sigma_y^2(\tau)$, abbreviated as MVAR, that includes an additional phase averaging operation, may be defined as:

$$Mod\,\sigma_y^2(\tau) = \frac{1}{2(N-3m+1)m^2\tau^2} \sum_{j=1}^{N-3m+1} \left[\sum_{i=j}^{m+j-1} \Big(x_{i+2m} - 2x_{i+m} + x_i\Big)\right]^2 \tag{24}$$

In contrast to the simple AVAR, MVAR too calculates the $\bar{y}_k$ values for all the overlapping windows, and not just for the adjacent windows, available in the dataset. One key distinction that can be noted between MVAR and AVAR is that MVAR measures the $\bar{y}_k$ values with a triangular weight function, in contrast to the uniform average in the case of AVAR, and it typically results in lower values as compared to AVAR. Due to the additional averaging operation, MVAR can distinguish between the white PM, flicker PM, and blue PM noise processes, which will be discussed in the next section, whereas AVAR cannot [6].

4) Time Variance: Allan variance and modified Allan variance are frequency stability measures averaged over the interval τ and hence, are measures of error per unit time. Time variance, abbreviated as TVAR, on the other hand, is an accumulated error over time, without the τ scaling factor in (19), and therefore has units of time. TVAR can be computed from modified Allan variance as:

$$TVAR = \sigma_x^2(\tau) = \Big(\frac{\tau^2}{3}\Big)\, Mod\,\sigma_y^2(\tau) \tag{25}$$

Thus the slope of TVAR is increased by a factor of 2 than the MVAR, and it is scaled down by 3, or in the case of deviations, the slope of TDEV is increased by 1, and it is scaled down by $\sqrt{3}$ as compared to MDEV [6], [23].

TABLE I: Characteristic slopes of different noise processes for various frequency and time domain stability measures [6].

Noise Process	Slope characteristics of the log-log plot				
	Frequency domain		Time domain		
	$S_y(f)$	$S_\phi(f)$ or $S_x(f)$	$\sigma_y^2(\tau)$	$\sigma_y(\tau)$	Mod $\sigma_y(\tau)$
	α	β	μ	$\mu/2$	$\mu^{'}/2$
Random Walk FM	-2	-4	1	1/2	1/2
Flicker FM	-1	-3	0	0	0
White FM	0	-2	-1	-1/2	-1/2
Flicker PM	1	-1	-2	-1	-1
White PM	2	0	-2	-1	-3/2
Blue PM	3	1	-2	-1	-2

III. Noise Processes and Conversion Methods

Most oscillators demonstrate distinct regions in their PSD profile with f^α dependence on frequency, commonly termed as noise processes. The total phase noise of an oscillator can be modeled using the sum of six such noise processes:

$$S_y(f) = \sum_{n=-2}^{+3} h_\alpha f^\alpha \tag{26}$$

wherein, h_α is the amplitude of the noise process and α is the slope of its frequency dependence when represented on a log-log plot. Since fluctuations in frequency and time can be related as $\frac{\Delta f}{f} = -\frac{\Delta t}{T}$ [24], these noise processes also show distinct slopes in their dependence on the measurement interval τ, represented as τ^μ in a log-log plot of Allan variance, or $\tau^{\frac{\mu}{2}}$, in the log-log plot of Allan deviation. Table I gives the coefficients for different noise processes and Fig. 4 shows some of these processes in both frequency and time domains. As mentioned in the previous section, modified Allan variance can distinguish between flicker PM, white PM, and blue PM noise processes, whereas, simple Allan variance cannot. The manifestation of different noise processes depends on a number of factors such as the technology used, oscillator topology, etc. Not all oscillators show all noise processes and the ability to measure these may also be limited by the hardware used.

A. Conversion Methods

The frequency and time domain stability measures can be converted amongst each other. To convert the PSD of fractional frequency fluctuations $S_y(f)$ into AVAR/MVAR, it must be multiplied by an appropriate windowing function $|H(f)^2|$, due to the averaging nature of $\bar{y}_k$, and integrated over the system bandwidth f_h. The averaging operation over τ in (19), behaves as a filter with the transfer function [6], [25]:

$$|H(f)|^2 = \frac{2(sin^4\pi f\tau)}{(\pi f\tau)^2} \tag{27}$$

Therfore, AVAR can be computed from $S_y(f)$ using (28) [6], [25].

$$\sigma_y^2(\tau) = 2\int_0^{f_h} S_y(f)\frac{sin^4(\pi f\tau)}{(\pi f\tau)^2} df \tag{28}$$

Alternatively, if the noise data is available in the form of noise processes, it can also be calculated using (29) [6].

$$\sigma_y^2(\tau) = h_{-2}\frac{(2\pi)^2}{6}\tau + h_{-1}2ln2 + h_0\frac{1}{2\tau} + h_1\frac{3\gamma - ln2 + 3ln(2\pi f_h\tau)}{(2\pi)^2\tau^2} + h_2\frac{3f_h}{(2\pi)^2\tau^2} + h_3\frac{3f_h^2}{2(2\pi)^2\tau^2} \quad (29)$$

wherein, $\gamma \approx 0.5772$, and f_h is the high frequency cutoff of a brick wall filter such that $f_h\tau = 1$, and h_{-2} - h_3 are the coefficients of translation available in [6]. Similarly, MVAR can be computed using (30) [6], [25]:

$$Mod\,\sigma_y^2(\tau) = 2\int_0^{f_h} S_y(f)\frac{sin^6(\pi f\tau)}{(m\pi f\tau)^2 sin^2(\frac{\pi f\tau}{m})}df \quad (30)$$

Phase noise can also be converted into jitter by integrating as given in (31) [26]. If the phase noise data is available in the form of noise processes, the integration can also be performed in a piece-wise manner as demonstrated in [27].

$$\sigma_{jitt} = \frac{1}{2\pi f_0}\sqrt{\int_{f_1}^{f_2} S_\phi(f)df} \quad (31)$$

Note that the frequency domain measures tend to have limitations when measuring at low frequency offsets. The time domain measures can provide better estimates for large τ values, which would be the time domain equivalent of the low frequency ranges. Moreover, while converting between different types of frequency stability measures, some information may be lost due to integration. Nonetheless, these are all different perspectives of the same phenomenon, noise-induced fluctuations in the frequency of an oscillator, and should be used together.

IV. Conclusion

A clear understanding of frequency stability is crucial when designing free-running oscillators for crystal-free IoT motes, especially if designing for communication standards such as IEEE 802.15.4 and BLE. In this paper, the fundamental metrics of frequency stability of oscillators, including frequency domain measures such as phase noise, and time domain measures such as Allan variance and jitter, are discussed. The conversion methods between frequency and time domains, as well as the power law dependence of various noise processes are also covered. By elaborating on these measures, the paper aids designers in understanding frequency stability nuances, empowering them to optimize oscillator designs effectively.

References

[1] "IEEE Standard for Local and metropolitan area networks–Part 15.4: Low-Rate Wireless Personal Area Networks (LR-WPANs)," *IEEE Std 802.15.4-2011 (Revision of IEEE Std 802.15.4-2006)*, pp. 1–314, 2011.

[2] "Bluetooth specification, core system package, low energy controller volume, journal = Bluetooth Core Specification v5.0," pp. 2533–2790, Dec. 2016.

[3] A. Hajimiri and T. Lee, "A General Theory of Phase Noise in Electrical Oscillators," *IEEE Journal of Solid-State Circuits*, vol. 33, no. 2, pp. 179–194, 1998.

[4] M. R. Khanzadi, D. Kuylenstierna, A. Panahi, T. Eriksson, and H. Zirath, "Calculation of the Performance of Communication Systems From Measured Oscillator Phase Noise," *IEEE Transactions on Circuits and Systems I: Regular Papers*, vol. 61, no. 5, pp. 1553–1565, 2014.

[5] D. C. Burnett, B. Wheeler, L. Lee, F. Maksimovic, A. Sundararajan, O. Khan, and K. S. J. Pister, "CMOS oscillators to satisfy 802.15.4 and Bluetooth LE PHY specifications without a crystal reference," in *2019 IEEE 9th Annual Computing and Communication Workshop and Conference (CCWC)*, 2019, pp. 0218–0223.

[6] "IEEE Standard Definitions of Physical Quantities for Fundamental Frequency and Time Metrology–Random Instabilities," *IEEE Std 1139-2022 (Revision of IEEE Std 1139-2008)*, pp. 1–60, 2022.

[7] B. Verhoef, J. Prummel, W. Kruiskamp, and R. Post, "18.6 A 32MHz Crystal Oscillator with Fast Start-up Using Synchronized Signal Injection," in *2019 IEEE International Solid-State Circuits Conference - (ISSCC)*, 2019, pp. 304–305.

[8] D. C. Burnett, F. Maksimovic, B. Wheeler, O. Khan, A. M. Niknejad, and K. S. Pister, "Free-running 2.4GHz Ring Oscillator-Based FSK TX/RX for Ultra-Small IoT Motes," in *2020 15th European Microwave Integrated Circuits Conference (EuMIC)*, 2021, pp. 101–104.

[9] L. B. Oliveira, J. R. Fernandes, M. M. Silva, I. Filanovsky, and C. Verhoeven, "Experimental Evaluation of Phase-Noise and Quadrature Error in a CMOS 2.4 GHz Relaxation Oscillator," in *2007 IEEE International Symposium on Circuits and Systems (ISCAS)*, pp. 1461–1464.

[10] R. Smith and T. Lee, "Analysis and Design of a Tetrahedral Oscillator," *IEEE Transactions on Circuits and Systems-II: Express Briefs*, vol. 69, no. 1, pp. 75–79, 2021.

[11] R. Navid, T. Lee, and R. Dutton, "Minimum achievable phase noise of RC oscillators," *IEEE Journal of Solid-State Circuits*, vol. 40, no. 3, pp. 630–637, 2005.

[12] J. Jalil, M. B. I. Reaz, and M. A. M. Ali, "CMOS Differential Ring Oscillators: Review of the Performance of CMOS ROs in Communication Systems," *IEEE Microwave Magazine*, vol. 14, no. 5, pp. 97–109, 2013.

[13] A. Abidi, "Phase Noise and Jitter in CMOS Ring Oscillators," *IEEE Journal of Solid-State Circuits*, vol. 41, no. 8, pp. 1803–1816, 2006.

[14] B. Razavi, *RF Microelectronics*. Pearson Education, 2011.

[15] D. B. Leeson, "Oscillator Phase Noise: A 50-Year Review," *IEEE Transactions on Ultrasonics, Ferroelectrics, and Frequency Control*, vol. 63, no. 8, pp. 1208–1225, 2016.

[16] G. Li and E. Afshari, "A Low-Phase-Noise Multi-Phase Oscillator Based on Left-Handed LC-Ring," vol. 45, no. 9, pp. 1822–1833.

[17] H. Q. Liu, W. L. Goh, L. Siek, W. M. Lim, and Y. P. Zhang, "A Low-Noise Multi-GHz CMOS Multiloop Ring Oscillator With Coarse and Fine Frequency Tuning," vol. 17, no. 4, pp. 571–577.

[18] E. Hegazi, H. Sjoland, and A. Abidi, "A filtering technique to lower LC oscillator phase noise," *IEEE Journal of Solid-State Circuits*, vol. 36, no. 12, pp. 1921–1930, 2001.

[19] S. A.-R. Ahmadi-Mehr, M. Tohidian, and R. B. Staszewski, "Analysis and Design of a Multi-Core Oscillator for Ultra-Low Phase Noise," vol. 63, no. 4, pp. 529–539.

[20] D. Batista, L. B. Oliveira, and I. Filanovsky, "Design of Ultra Low Power CMOS Oscillators Using Active Inductors," in *2021 IEEE International Midwest Symposium on Circuits and Systems (MWSCAS)*. Lansing, MI, USA: IEEE, 2021, pp. 141–145. [Online]. Available: https://ieeexplore.ieee.org/document/9531816

[21] N. Da Dalt and A. Sheikholeslami, *Understanding Jitter and Phase Noise: A Circuits and Systems Perspective*. Cambridge University Press, 2018.

[22] D. Allan, "Statistics of atomic frequency standards," *Proceedings of the IEEE*, vol. 54, no. 2, pp. 221–230, 1966.

[23] W. J. Riley, W. J. Riley, and J. A. Barnes, "Handbook of frequency stability analysis." NIST, 2008.

[24] R. Solis, "Time and Frequency Metrology: Fundamental concepts in Time and Frequency metrology." [Online]. Available: https://www.nist.gov/system/files/documents/iaao/TyF-talk-final_Raul-Solis.pdf

[25] D. Allan, "Conversion of Frequency Stability Measures from the Time-domain to the Frequency-domain, vice-versa and Power-law Spectral Densities," Jan. 2012.

[26] Y. Zhao and B. Razavi, "Phase Noise Integration Limits for Jitter Calculation," in *2022 IEEE International Symposium on Circuits and Systems (ISCAS)*. Austin, TX, USA: IEEE, May 2022, pp. 1005–1008.

[27] W. Kester, "Converting Oscillator Phase Noise to Time Jitter," 2005. [Online]. Available: https://www.analog.com/media/en/training-seminars/tutorials/MT-008.pdf